Journal of Marine Science and Technology

Volume 20 | Issue 5 Article 13

# OPTIMAL DYNAMIC TEMPORAL-SPATIAL PARAMTER INVERSION METHODS FOR THE MARINE INTEGRATED ELEMENT WATER QUALITY MODEL USING A DATA-DRIVEN NEURAL NETWORK

Ming-Chang Li
*Laboratory of Environmental Protection in Water Transport Engineering, Tianjin Research Institute of Water Transport Engineering, Tianjin, China.*, lmcsq1997@163.com

Shu-Xiu Liang
*State Key Laboratory of Coastal and Offshore Engineering, Dalian University of Technology, Dalian, China.*

Zhao-Chen Sun
*State Key Laboratory of Coastal and Offshore Engineering, Dalian University of Technology, Dalian, China.*

Guang-Yu Zhang
*Laboratory of Environmental Protection in Water Transport Engineering, Tianjin Research Institute of Water Transport Engineering, Tianjin, China.*

# OPTIMAL DYNAMIC TEMPORAL-SPATIAL PARAMTER INVERSION METHODS FOR THE MARINE INTEGRATED ELEMENT WATER QUALITY MODEL USING A DATA-DRIVEN NEURAL NETWORK

## Acknowledgements

The present work was supported by the National Natural Science Foundation of China (No. 51209110), the National Nonprofit Institute Research Grants of TIWTE (TKS090204, TKS100217 and KJFZJJ2011-01), the Research Foundation of State Key Laboratory of Coastal and Offshore Engineering Dalian University of Technology (LP1108) and the project of Science and Technology for Development of Ocean in Tianjin (KJXH2011-17).

*Journal of Marine Science and Technology, Vol. 20, No. 5, pp. 575-583 (2012)*
DOI: 10.6119/JMST-012-0109-1


# OPTIMAL DYNAMIC TEMPORAL-SPATIAL PARAMTER INVERSION METHODS FOR THE MARINE INTEGRATED ELEMENT WATER QUALITY MODEL USING A DATA-DRIVEN NEURAL NETWORK

Ming-Chang Li[1], Shu-Xiu Liang[2], Zhao-Chen Sun[2], and Guang-Yu Zhang[1]

Key words: artificial neural network (ANN), data-driven model, integrated element, marine water quality model, temporal-spatial inversion.

## ABSTRACT

Certain marine water quality or ecosystem model parameters vary in space and time because of different plankton taxonomic compositions over a large domain. The same parameter vectors can result in suboptimal calibration. In the present paper, a data-driven model based on an artificial neural network is developed to inverse the values of model parameters dynamically. All training data used are calculated using numerical water quality models from the results of multi-parameter matching design cases such that physical properties are not disturbed. The aim is to determine the relationship between the model parameters and the pollution concentration values of interior stations. Field data are used in the analysis of the relationship for inversing optimal parameters. The temporal and spatial variations of sensitive parameters are considered using four inversion methods, namely, temporal-spatial, spatial, temporal and non-temporal, and non-spatial, to enhance the model accuracy. In water quality models, an integrated element method is simultaneously applied using grids for spatial variation. Case studies in the Bohai Sea, China, and an identical experiment using dissolved inorganic nitrogen are conducted to validate the aforementioned methods. The average maximum of absolute error is reduced from 0.0435 to 0.00756, with a reduction rate of 82.62%. The results show that the temporal-spatial inversion method improves the accuracy of the water quality model.

*Paper submitted 11/12/10; revised 05/11/11; accepted 01/09/12. Author for correspondence: Ming-Chang Li (e-mail: lmcsq1997@163.com).*
*[1] Laboratory of Environmental Protection in Water Transport Engineering, Tianjin Research Institute of Water Transport Engineering, Tianjin, China.*
*[2] State Key Laboratory of Coastal and Offshore Engineering, Dalian University of Technology, Dalian, China.*

## I. INTRODUCTION

Marine water quality or ecosystem models are important in both the long-term prediction of the global climate and the short-term forecast of changes in the quality of basin-scale water [3]. However, a number of input conditions must be provided to enhance the accuracy of numerical modeling. One of the common features of marine water quality or ecosystem models is the presence of a large number of poorly known parameters, making direct measurement difficult, if not impossible. Therefore, the parameter qualification and model verification involved are significant in any event.

Since Shastry *et al*. [26] estimated the parameter of the biochemical oxygen demand-dissolved oxygen model, studies have focused on the optimization of the model parameter [2, 4, 15, 19, 29, 30]. Trial and error [7] is a widely used technique for model calibration [25]. However, the accuracy of this model completely depends on subjective experience. With the abundance of satellite data, data assimilation methods have been recently employed for model calibration, with the adjoint technique as the most commonly used method. Lawson *et al*. [13] introduced the adjoint method for data assimilation in a simple predator-prey model. The Lagrange operator method is employed to construct the adjoint equation, resulting in the successful estimation of the model parameter and initial field conditions. Subsequently, Lawson *et al*. [12] used this method in a complex marine ecosystem model that includes five state variables. With optimizations using synthetically produced data, they examined the necessary sampling rates to recover the parameter values of the model. Vallino [28] tested the capability of various data assimilation methods in incorporating mesocosm experimental data into a marine ecosystem model and established the numerical instability of the adjoint approach.

Sensitive model parameters vary in space and time because

of different plankton taxonomic compositions over a large domain [5, 23]. The same concept was adopted by Hemmings *et al*. [9, 10] and Losa *et al*. [16, 17]. Hemmings *et al*. [9] attempted to optimize parameter vectors over a large domain at multiple stations and found that deduction from a single parameter vector can result in suboptimal calibration. Subsequently, they implemented a new method for using ocean color data for spatial variation optimization [10]. Meanwhile, Losa *et al*. [16, 17] used different parameter vectors in separate domains in the North Atlantic to validate the ecosystem model. Their simulation indicated that the temporal and spatial variations of model parameters, rather than an improvement in the accuracy of the physical model, affect the state variable.

Optimal parameter estimation can be achieved through this technique, but both water quality model and adjoint equations need to be calculated. Adjoint equations are as complicated as water quality model equations because they require additional time for calibration. When applied in practical engineering, the adjoint technique results in numerous uncertainties attributable to the absence of field data in the calibrated model. Furthermore, the application of a data assimilation method is also limited [18].

The current paper aims to develop a practical technique for the optimal inversion of model parameters. Optimal parameters are inversed using a data-driven model [27] based on an artificial neural network. Four inversion methods, namely, temporal-spatial, spatial, temporal and non-temporal, and non-spatial, are then developed to improve the simulated accuracy of the water quality model. The Osaka Daigaku Estuary Model (ODEM) [22] is used to simulate the marine water quality in the involved areas.

The present work is organized as follows: In Section 2, the basic concepts of the data-driven model, the Back-Propagation Neural Network (BPNN), and the ODEM are introduced. Moreover, the detailed procedure on the inversion of model parameters and the four inversion methods are also discussed. The method is presented in Section 3 and verified using an entitative ocean in Section 4. Finally, the conclusions are given in Section 5.

## II. NUMERICAL MODELS

### 1. Data-Driven Model

Unlike physically based models, data-driven models rely purely on the limited knowledge of the modeling process and input and output data to describe system characteristics. The model makes abstractions and generalizations of the process and often complements the physically based model. Data-driven models can be implemented with ANNs, expert systems, fuzzy logic concepts, rule inductions, and machine learning systems. The fundamental expression of the data-driven model is as follows:

$$\left(y_1,\cdots,y_i,\cdots y_m\right)=F\left(x_1,\cdots,x_i,\cdots x_n\right) \tag{1}$$

$\left(x_1,\cdots,x_i,\cdots x_n\right)$ and $\left(y_1,\cdots,y_i,\cdots y_m\right)$ are the input and output variables, respectively, where m is the number of output variables, n is the number of input variables, and $F$ is the objective function that the model has to identify. In the current research, the results of ANN are used for the fitting of $F$.

### 2. Back-Propagation Neural Network

Since McCulloch and Pitts [20] introduced the concept of ANN, numerous models have been developed. The BPNN proposed by Rumelhart *et al*. [24] addressed the hidden layer of learning difficulty in multi-layer networks and became the most commonly used model among all ANNs. The key point is the discovery of the error in the back propagation technique. In the BPNN learning process, interconnection weights are adjusted from the back to the front layers to minimize output error. The main advantage of BPNN is that it can approach any nonlinear continuous function after being trained [11]. Several numerical details of the BPNN are described in the following section.

*1) Data Normalization*

All data of the input and output layers are normalized in a range from 0 to 1 using Eq. (2):

$$\bar{Y}_{gi}=\frac{Y_{gi}-Y_{g\min}}{Y_{g\max}-Y_{g\min}} \tag{2}$$

where $\bar{Y}_{gi}$ and $Y_{gi}$ are the values of the data after and before normalization, respectively, and $Y_{g\max}$ and $Y_{g\min}$ are the maximum and minimum of all data, respectively.

To consider nonlinearity, the following sigmoid transfer function is used:

$$s(x)=1\Big/\left(1+e^{-x+\theta}\right) \tag{3}$$

where $\theta$ is the threshold value of hidden neurons.

*2) Learning Rate $\eta$ and Appended Momentum*

The efficiency and speed of convergence of the BPNN learning algorithm are affected by the learning rate $\eta$ and the appended momentum (L&A). L&A refers to the control parameters of BPNN training algorithms and control the step size when weights are iteratively adjusted. A low L&A results in a slow learning by the network, whereas a high L&A results in the divergence of the weights and objective function, so learning is nil. The value of L&A depends on whether the time series changes frequently. If it does, the value of L&A should be increased. In the present work, the L&A ranges from 0 to 1, the learning rate is set to 0.05, and the appended momentum is 0.5 after testing.

*3) Error Function*

The root mean squared error (RMSE) is used to evaluate the accuracy of prediction and is defined as follows:

$$RMSE = \sqrt{\sum_{i=1}^{n}(Y_i - Y_i^{'})^2 \Big/ n} \tag{4}$$

where $n$ is the number of data, $Y_i$ is the value of the field data, and $Y_i^{'}$ is the value predicted by the neural network.

The correlation coefficient (CC) is computed using Eqs. (5)-(7). The maximum of absolute error (MAE) and the maximum of relative error (MRE) are calculated using Eqs. (8)-(9).

$$CC = \frac{\sum_{i=1}^{n}\left(\eta_i^o - \overline{\eta}^o\right)\left(\eta_i^p - \overline{\eta}^p\right)}{\sqrt{\sum_{i=1}^{n}\left(\eta_i^o - \overline{\eta}^o\right)^2 \sum_{i=1}^{n}\left(\eta_i^p - \overline{\eta}^p\right)^2}} \tag{5}$$

$$\overline{\eta}^o = \frac{\sum_{i=1}^{n}\eta_i^o}{n} \tag{6}$$

$$\overline{\eta}^p = \frac{\sum_{i=1}^{n}\eta_i^p}{n} \tag{7}$$

$$MAE = MAX\left[\left|\eta_i^o - \eta_i^p\right|_{i=1}^{n}\right] \tag{8}$$

$$MRE = MAX\left[\left|\frac{\eta_i^o - \eta_i^p}{\eta_i^o}\right|_{i=1}^{n}\right] \tag{9}$$

where CC is the correlation coefficient, $\eta^o$ is the field data, $\eta^p$ is the simulated data, and $n$ is the number of data. The overbar, MAE, and MRE indicate the mean value, maximum of absolute errors, and maximum of relative errors, respectively.

*4) Structure of the Neural Network*

The structure of the neural network, including the number of hidden layers and neurons, is determined by the complexity of the problem to be solved. An increase in the number of hidden layers and neurons can reflect the complexity of the problem and decrease the number of iteration steps. However, this relationship is not useful in increasing precision and may result in overfitness [21]. Therefore, one hidden layer is used in the present paper.

The number of neurons for the hidden layer can be calculated using the following formula:

$$NH = \frac{NI + NO}{2} \tag{10}$$

where *NH*, *NI*, and *NO* are the numbers of neurons in the hidden, input, and output layers, respectively. More detailed information can be found in the work of Li *et al*. [14].

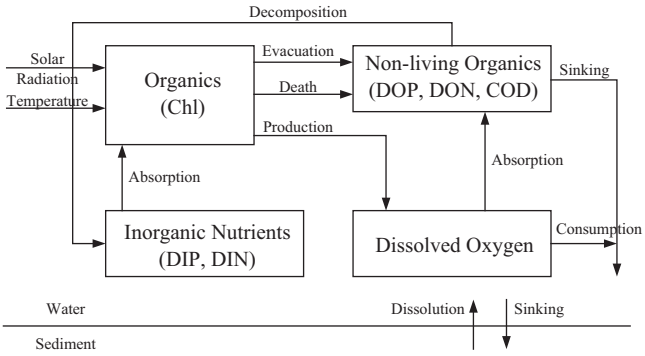


**Fig. 1. Schematic diagram of matter circulation in the ODEM.**

## 3. Marine Integrated Element Water Quality Model (MIEWQM)

A water quality model is the fundamental simulation tool for regional water environmental management. Such a model attempts to explain the underlying physical-biochemical processes. A number of water quality models can retrieve entitative ocean conditions with high precision. Complex models that include details on the physical-biochemical processes have become possible because of the rapid increase of computing capability. However, excessive complexity inevitably results in numerous uncertainties and problems in the interpretation of the dynamics process of the model [1]. ODEM, developed by Nakatuji is employed as a water quality simulation tool to validate optimal dynamic temporal and spatial parameter inversion. ODEM has been used not only for water quality modeling, but also for coastal water studies. The sensitive model parameters are not constant, but may vary in space and time because of different plankton taxonomic compositions over a large domain. Therefore, the split-domain and period parameter evaluation method, called MIEWQM, is presented in this model.

Fig. 1 shows the schematic diagram of matter circulation in ODEM. Phytoplanktons release nonliving organics (e.g., organic nitrogen, organic phosphorus, and chemical oxygen demand) and dissolve oxygen by evacuation, death, and production. Parts of the nonliving organics sink into the sediment with detritus, and others decompose into inorganic nutrients combined with dissolved oxygen. Phytoplankton growth is controlled by inorganic nutrients, temperature, and solar radiation.

# III. OPTIMAL DYNAMIC TEMPORAL AND SPATIAL PARAMTER INVERSION METHOD

A new technique that automatically combines a data-driven model with the water quality model was developed. In this technique, the water quality model repeats a series of designed computations. Subsequently, a data set containing the corresponding relationship between the values of the model parameters [$(x_1, \ldots, x_i, \ldots x_n)$ in Eq. (1)] and the values of interior stations for pollution (state variables) [$(y_1, \cdots, y_i, \cdots y_m)$ in Eq.

(1)] is stored. The task of the data-driven model is to determine the relationship [$F$ in Eq. (1)] between ($x_1$, …, $x_i$, … $x_n$) and ($y_1$, …, $y_i$, … $y_m$). After the field data are transferred into the model, values of the optimal model parameter are inverted. The detailed procedure of the technique and the temporal and spatial inversion methods are given below.

## 1. Detailed Inversion Procedure

*Step 1: Selection of control variables*

Various parameters in the water quality model react differently with one another. If all forms are included, the computation cost becomes excessive, and uncertainty increases [6]. Therefore, sensitive model parameters have been analyzed to select the control variables [8].

*Step 2: Case computation using the water quality model*

In water quality numerical models, the governing equations have to be discretized into the computation domain. Initial guess values for all controlled variables are assumed, and their corresponding ranges are set. If the number of controlled variables is m, and n values are taken for one control variable, as many as $\prod_{i=m}\left[C_n^1\right]_i = n^m$ designed cases are obtained. All designed cases are individually computed using ODEM. The results of pollution concentration serve as output and are stored for the data-driven model.

*Step 3: Model parameter inversion using the data-driven model*

The results of pollution concentrations in interior stations and the values of their corresponding parameters are inputted into the data-driven model. After training, the relationship between the interior stations and the model parameters is generalized. To obtain the optimal solution, the field data on interior stations are inputted into the abovementioned relationship.

*Step 4: Verification of the optimal solution*

The optimal solution in the water quality model is inputted, and the computation is repeated. The RMSE between the measurement and the results of the numerical computation is calculated.

Fig. 2 describes the process of model parameter inversion. The sequence is denoted from 1 to 8. Two modules are used in the entire process, namely, water quality and optimal inversion. The computation of the designed cases and the final verification are performed by the water quality module. The optimal inversion module is responsible for the analysis of the water quality model results, as well as the generalization of the relationship between the model parameters and the interior stations. The database of the two modules comprises A and B.

## 2. Temporal-spatial Inversion Methods (TSIM)

Over a large simulating region, the model parameters are affected by various factors that have temporal and spatial differences. The model parameter set in every grid and time

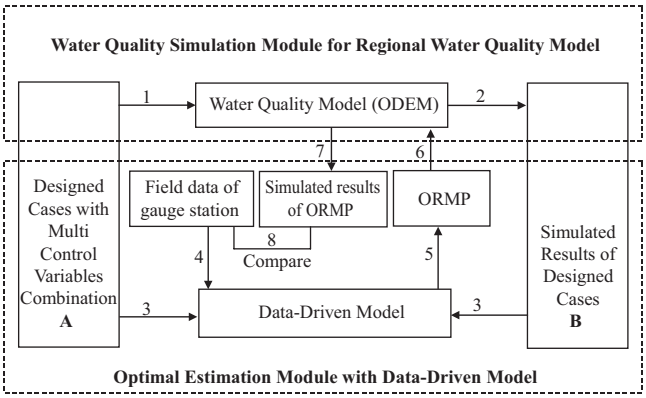


Note: ORMP: Optimal Resolution of Model Parameter

**Fig. 2. Diagram of optimal estimation of model parameter using data-driven model combined with water quality model.**

step ($a = a(x, y, z, t)$) is efficient in improving model precision. Excessive details result in numerous uncertainties and time-consuming problems. The split-domain method is determined by geographical position, longitudinal-latitudinal scope, and observed sites. The variation period in time is divided into days, months, or seasons by the entire simulating period and the continuous or discrete characteristics of the validated data. If the number of elements is $N$, and the time segments are $M$, the parameter $a$ is set to $a_{j\to1,N}^{i\to1,M}$ in the model. The relationship of the interior stations and the model parameters is generalized using the data-driven model of Step 3 [Eq. (11)]. The optimal solution of the model parameters $\left[a_{j\to1,N}^{i\to1,M}, b_{j\to1,N}^{i\to1,M}, \cdots, z_{j\to1,N}^{i\to1,M}\right]'$ is obtained by inputting field data on interior stations into the above relationship.

$$\begin{bmatrix} a_1, b_1, \cdots, z_1 \\ a_2, b_2, \cdots, z_2 \\ \cdots \\ a_N, b_N, \cdots, z_N \end{bmatrix}^{i\to(1,M)} = F_1^{i\to(1,M)} \begin{bmatrix} St_1^1(t), St_1^2(t), \cdots, St_1^k(t) \\ St_2^1(t), St_2^2(t), \cdots, St_2^k(t) \\ \cdots \\ St_N^1(t), St_N^2(t), \cdots, St_N^k(t) \end{bmatrix}^{i\to(1,M)} \tag{11}$$

where ($a$, $b$, …, $z$) are the model parameters, $St$ is the state variable, the superscript $k$ is the number of state variables, the subscript $N$ is the number of elements, $F_1^i$ is the relationship of the $i$th time period, and $t$ is the time step of the model output data in the $i$th time period.

The network structure of integrated element model parameter temporal-spatial inversion is shown in Fig. 3.

In Fig. 3, a three-layer neural network is designed to inverse the model parameters, where $T$ stands for the entire simulating period. The input layer is the pollution concentrations in the interior stations in each element, and the output layer is the model parameters.

In validating the superiority of the temporal-spatial

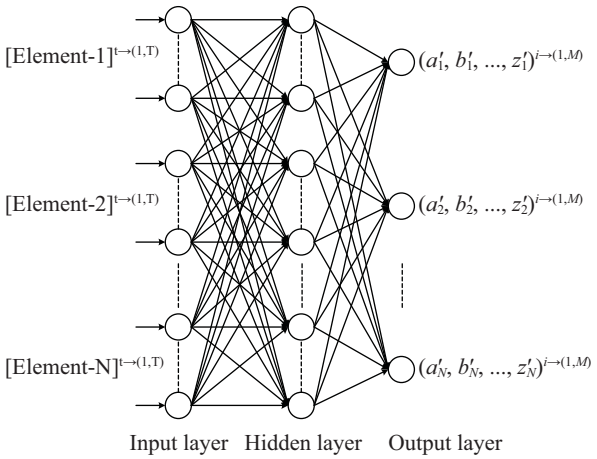


**Fig. 3. Network structure of integrated element model parameter temporal-spatial inversion using the data-driven model.**

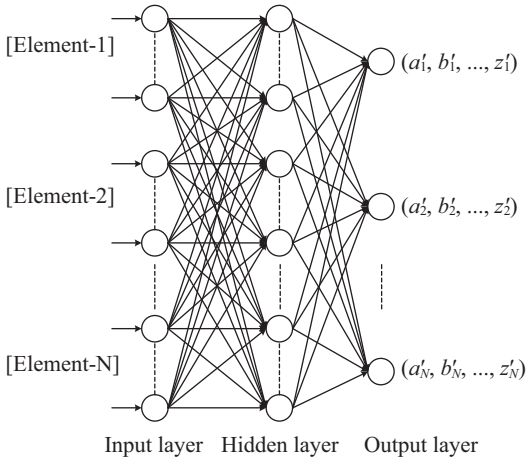


**Fig. 4. Network structure of integrated element model parameter spatial inversion using the data-driven model.**

inversion method, three methods are used, namely, the spatial, temporal and non-temporal, and non-spatial inversions. The inversion procedures of the three methods are the similar to that of temporal-spatial inversion.

Time variation is disregarded in the spatial inversion method (SIM), so the relationship of interior stations and the model parameters is generalized using the data-driven model of Step 3 in Eq. (12). The optimal solution of the model parameters $\left[a_{j\to 1,N}, b_{j\to 1,N}, \cdots, z_{j\to 1,N}\right]'$ is obtained by inputting the field data of interior stations. The network structure of the spatial inversion of the integrated element model parameter is shown in Fig. 4.

$$\begin{bmatrix} a_1, b_1, \cdots, z_1 \\ a_2, b_2, \cdots, z_2 \\ \cdots \\ a_N, b_N, \cdots, z_N \end{bmatrix} = F_2 \begin{bmatrix} St_1^1, St_1^2, \cdots, St_1^k \\ St_2^1, St_2^2, \cdots, St_2^k \\ \cdots \\ St_N^1, St_N^2, \cdots, St_N^k \end{bmatrix} \tag{12}$$

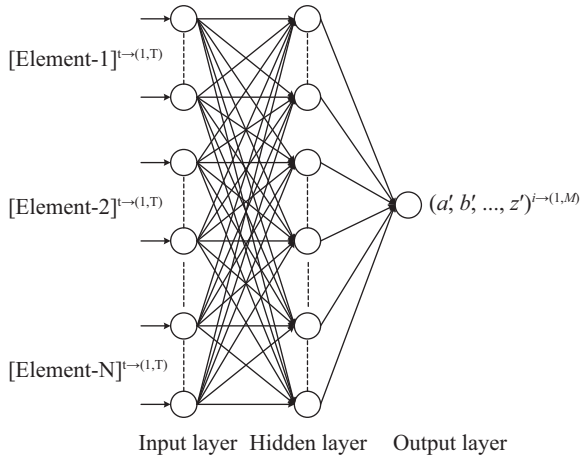


**Fig. 5. Network structure of integrated element model parameter temporal inversion using the data-driven model.**

Space variation is also ignored in the temporal inversion method (TIM), so the relationship of interior stations and the model parameters is generalized using the data-driven model of Step 3 in Eq. (13). The optimal solution of the model parameters $\left[a^{i\to 1,M}, b^{i\to 1,M}, \cdots, z^{i\to 1,M}\right]'$ is obtained by inputting the field data on interior stations. The network structure of the temporal inversion of the model parameter is shown in Fig. 5.

$$\left[a, b, \cdots, z\right]^{i\to(1,M)} = F_3^{\,i\to(1,M)}\left[St^1(t), St^2(t), \cdots, St^k(t)\right]^{i\to(1,M)} \tag{13}$$

Space and time variations are disregarded in the non-temporal and non-spatial inversion methods (NTNSIM), so the relationship between interior stations and the model parameters is generalized using the data-driven model of Step 3 in Eq. (14). The optimal solution of the model parameters $\left[a, b, \cdots, z\right]'$ is obtained by inputting the field data on interior stations. The network structure of the non-temporal and non-spatial inversions of the model parameter is shown in Fig. 6.

$$\left[a, b, \cdots, z\right] = F_4\left[\left(St^1, St^2, \cdots, St^k\right)\right] \tag{14}$$

## IV. CASE STUDIES

Case tests were performed in the Bohai Sea, China, which is a semiclosed sea with a mean depth of 18.7 m and an area of more than 80 000 km$^2$. The bottom of this sea is very flat, with an average slope of 28". Fig. 7 shows the location of the research region and the corresponding elements. The whole sea is divided into four elements by geographical position, namely, Laizhou Bay (LzB), Bohai Bay (BhB), Liaodong Bay (LdB), and the opposite area. Three gauge stations are chosen,

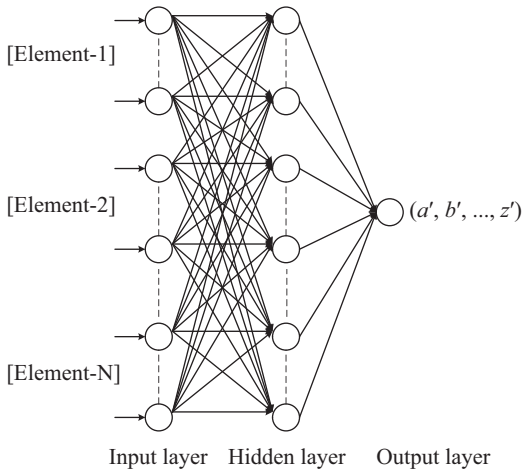


**Fig. 6. Network structure of integrated element model parameter non-temporal and non-spatial inversion using the data-driven model.**

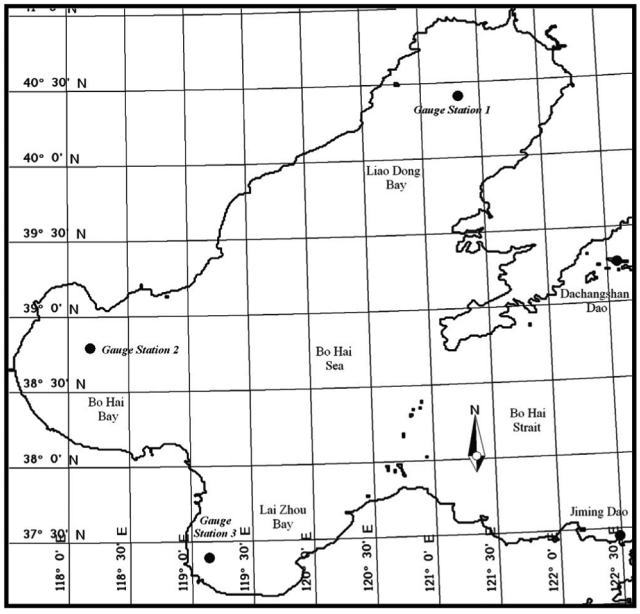


**Fig. 7. Locations of the research regions and the corresponding elements.**

namely, those in Laizhou, Bohai, and Liaodong Bays. The locations of the gauge stations are shown in Table 1, so the number of elements is 3 ($N$ = 3).

In the numerical simulation, the area was discretized as 4 km × 4 km horizontally and 17 levels in depth. To lessen computational time and improve accuracy, the level thickness was varied (i.e., nonuniform) based on water depth. The level thickness was 4 m × 1, 2 m × 4, 3 m × 5, 4 m × 3, 5 m × 2, and 6 m × 2 from top to bottom. The model time step is 30 s. The surface height along the open boundary is given by interpolating the results between Dachangshan Dao (39°16'N, 122°35′E) and Jiming Dao (37°27′N, 122°35′E). Five primary tidal constituents, namely, $M_2$, $S_2$, $K_1$, $O_1$, and $N_2$, are inputted in two open boundary control stations.

**Table 1. Elements and locations of gauge stations.**

| Element | Gauge station | Coordinate | |
|---|---|---|---|
| | | Longitude | Latitude |
| LdB | 1 | 121°19′12″E | 40°24'31″N |
| BhB | 2 | 118°10′54″E | 38°47'36″N |
| LzB | 3 | 119°08′30″E | 37°23'36″N |

**Table 2. State variables and sensitive parameters.**

| State variable | Sensitive parameters | Unit |
|---|---|---|
| DIN | Growth rate of phytoplankton (VMMAX) | 1/d |
| | Growth temperature of phytoplankton (TEMPS) | °C |
| | Decomposed rate of DIN (DRDN) | 1/d |

**Table 3. Values of sensitive parameters.**

| State variable | Sensitive parameter | Values | | |
|---|---|---|---|---|
| DIN | VMMAX | 1.44 | 2.5 | 3.36 |
| | TEMPS | 15 | 26 | 35 |
| | DRDN | 0.012 | 0.018 | 0.026 |

## 1. Choices of the Control Variable

As the state variable, dissolved inorganic nitrogen (DIN) is considered to verify the present inversion methods. The coefficient of variation is computed using the Monte Carlo method [8] to validate the sensitivity of the model parameters. The state variable and its sensitive parameters are listed in Table 2.

In Table 2, DIN has three sensitive parameters. The corresponding ranges of the control variables are set among the initial guess values in Table 3.

In Table 3, the values of the control variables are listed. For each control variable, three values are taken in its range, and 27 designed cases are obtained.

## 2. Optimal Inversion Using the four Methods

A total of 27 cases of pollution concentration data of 144 h are acquired 27 times by the water quality model computation. After inputting the 27 DIN data of 144 h and the relative sensitive parameter data in Table 3 into the data-driven model of the four methods, the relationships are generalized.

The entire simulation period of the water quality model lasted for 144 h ($T$ = 144), which was divided into six time segments by day ($M$ = 6).

In the present paper, the purported "identical twin experiment" method [6] is used to verify the efficiency of the four inversion methods.

The parameters in Table 4 are utilized as real values and are inputted into ODEM for the pollution concentration data as pseudo-field data. The optimal model parameters in Table 5 are inversed by inputting the pseudo-field data into the above-mentioned relationships.

**Table 4. Design of identical twin experiment.**

| State variable | Sensitive parameter | | |
|---|---|---|---|
| DIN | VMMAX | TEMPS | DRDN |
| | 2.4 | 25 | 0.02 |

**Table 5. Optimal solutions of control variables.**

| Methods | Space | Day | Sensitive parameters | | |
|---|---|---|---|---|---|
| | | | VMMAX | TEMPS | VKDN |
| TSIM | LdB | 1 | 2.542602 | 27.03175 | 0.018688006 |
| | | 2 | 2.540686 | 27.53403 | 0.018687641 |
| | | 3 | 2.540865 | 26.53339 | 0.018678859 |
| | | 4 | 2.539487 | 25.95475 | 0.018675916 |
| | | 5 | 2.538764 | 25.59593 | 0.018670041 |
| | | 6 | 2.536907 | 25.63993 | 0.018675208 |
| | BhB | 1 | 2.540225 | 27.4360 | 0.018688262 |
| | | 2 | 2.539396 | 27.2660 | 0.018687986 |
| | | 3 | 2.536939 | 25.58158 | 0.01867817 |
| | | 4 | 2.542715 | 25.22310 | 0.018660115 |
| | | 5 | 2.543290 | 25.17976 | 0.018658930 |
| | | 6 | 2.537674 | 25.52926 | 0.018681202 |
| | LzB | 1 | 2.541938 | 27.49997 | 0.018688086 |
| | | 2 | 2.539326 | 27.27622 | 0.018687652 |
| | | 3 | 2.540275 | 25.32287 | 0.018675525 |
| | | 4 | 2.540646 | 25.45963 | 0.018670442 |
| | | 5 | 2.542415 | 25.19416 | 0.018658789 |
| | | 6 | 2.537083 | 25.64511 | 0.018678861 |
| SIM | LdB | 6 days | 2.54429385 | 25.368715 | 0.019675208 |
| | BhB | | 2.4485965 | 25.037195 | 0.018655743 |
| | LzB | | 2.4929345 | 25.40553 | 0.020678861 |
| TIM | Bohai Sea | 1 | 2.5415883 | 27.3225733 | 0.018688118 |
| | | 2 | 2.5398027 | 27.3587500 | 0.018687760 |
| | | 3 | 2.5393597 | 25.8126133 | 0.018677518 |
| | | 4 | 2.5409493 | 25.5458267 | 0.018668824 |
| | | 5 | 2.5414897 | 25.3232833 | 0.018662587 |
| | | 6 | 2.5372213 | 25.6047667 | 0.018678424 |
| NTNSIM | Bohai Sea | 6 days | 2.527048 | 25.44823167 | 0.018669937 |

## 3. Verification of the Optimal Inversion Solutions

The final verification was implemented with the optimal solutions of the model parameters in Table 5 using the four inversion methods. The comparisons of the DIN calibration results are shown in Figs. 8-10. The RMSEs, CCs, MAEs, and MREs between the measurement and the results of the numerical computation are listed in Table 6.

Figs. 8-10 show the comparison of calibration results among the four inversion methods in the three elements. The temporal-spatial inversion method is superior to the other three based on the errors shown in Table 6, particularly in terms of peak scope. Certain model parameters have evident physical significance, such as the phytoplankton growth rate (VMMAX), which was synthetically affected by temperature, solar radiation, salinity, wind, and the regional ecosystem.

**Table 6. Errors of calibration results.**

| Space | Error | TSIM | SIM | TIM | NTNSIM |
|---|---|---|---|---|---|
| LdB | MAE | 0.00729 | 0.01481 | 0.03536 | 0.04345 |
| | MRE | 1.573% | 3.195% | 7.628% | 9.373% |
| | RMSE | 0.0027 | 0.0056 | 0.0136 | 0.0167 |
| | CC | 0.9999 | 0.9996 | 0.9977 | 0.9965 |
| BhB | MAE | 0.00827 | 0.01852 | 0.03795 | 0.04624 |
| | MRE | 1.772% | 3.968% | 8.131% | 9.907% |
| | RMSE | 0.0037 | 0.0088 | 0.0184 | 0.0225 |
| | CC | 0.9998 | 0.9991 | 0.9962 | 0.9943 |
| LzB | MAE | 0.00712 | 0.01368 | 0.03340 | 0.04081 |
| | MRE | 1.846% | 3.546% | 8.658% | 10.578% |
| | RMSE | 0.0025 | 0.0050 | 0.0125 | 0.0153 |
| | CC | 0.9998 | 0.9993 | 0.9954 | 0.9931 |

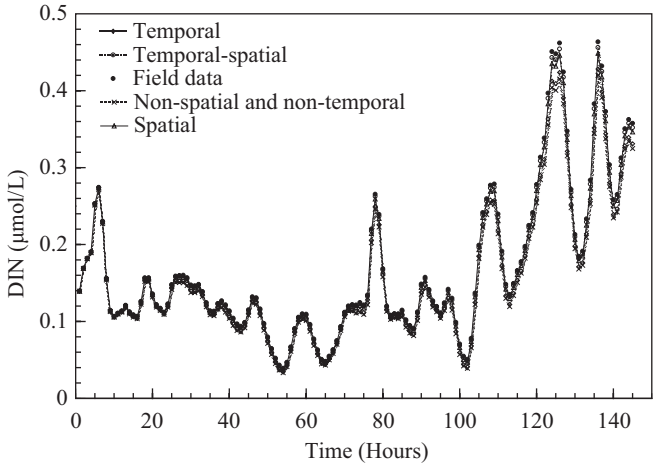


**Fig. 8. Comparison of DIN calibration results among the four inversion methods in Liaodong Bay.**

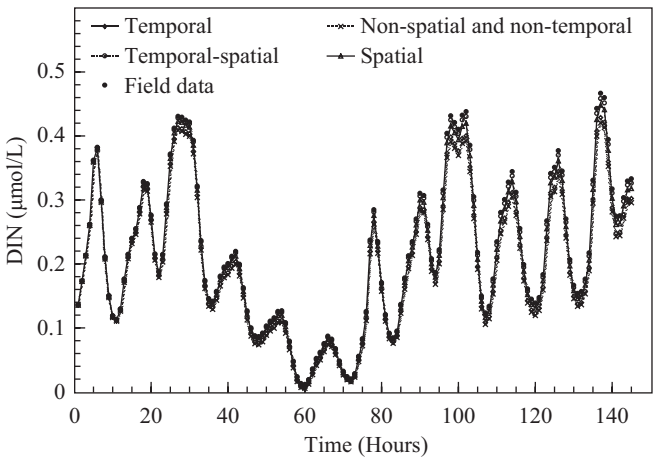


**Fig. 9. Comparison of DIN calibration results among the four inversion methods in Bohai Bay.**

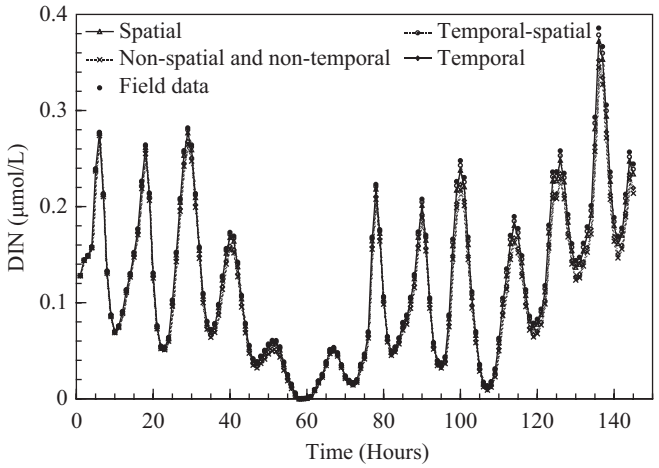


**Fig. 10. Comparison of DIN calibration results among the four inversion methods in Laizhou Bay.**

Temporal and spatial differences exist consequentially. These differences are ignored in the non-temporal and non-spatial method, which consequently has the lowest precision. The temporal inversion method requires balance within elements. Hence, the spatial inversion method is more suitable for multiple gauge station validation.

Compared with the adjoint method, the present methods have three key advantages. The first advantage is simplicity. The data-driven model based on BPNN is easy to develop, unlike complicated adjoint equations. The second advantage is flexibility. If the basic equations of the water quality model change, the adjoint equations reformulate accordingly. In the present method, the data-driven model can remain unchanged if different water quality models are used. Third, the present models are less time consuming. The adjoint technique repeats the computation for both water quality model and adjoint equations. Even with good initial guesses, additional time is consumed for adjoint equations compared with the present method.

## V. CONCLUSION

A new method has been developed to inverse the model parameter values. In this method, the data-driven and water quality models are automatically merged. The water quality model repeats a number of computations for designed cases, and the results of the pollution concentration data serve as the output and are stored for the data-driven model. The data-driven model generalizes the relationship between the model parameters and the interior stations. After the field data are imported, optimal solutions are obtained.

Four inversion methods, namely, temporal-spatial, spatial, temporal, and non-temporal and non-spatial, are developed to improve the simulated accuracy of the water quality model. The temporal-spatial inversion method is found to be superior to the others because of its comprehensive consideration of the temporal and spatial differences of the model parameters. Compared with the temporal inversion method, the spatial inversion method is more suitable for the validation of multiple gauge stations. Compared with the adjoint method, the presented methods are simpler, more flexible and less time consuming.

In a case study, the pseudo-field data of concentration are used to inverse the model parameters. The present inversion method is found to be suitable for the inverse problem.

## ACKNOWLEDGMENTS

The present work was supported by the National Natural Science Foundation of China (No. 51209110), the National Nonprofit Institute Research Grants of TIWTE (TKS090204, TKS100217 and KJFZJJ2011-01), the Research Foundation of State Key Laboratory of Coastal and Offshore Engineering Dalian University of Technology (LP1108) and the project of Science and Technology for Development of Ocean in Tianjin (KJXH2011-17).

## REFERENCES

1. Anderson, T., "Plankton functional type modelling: running before we can walk?," *Journal of Plankton Reserch*, Vol. 2, No. 11, pp. 1073-1081 (2005).
2. Arhonditsis, G. B., Paerl, H. W., Valdes-Weaver, L. M., Stow, C. A., Steinberg, L. J., and Reckhow, K. H., "Application of Bayesian structural equation modeling for examining phytoplankton dynamics in the Neuse River Estuary (North Carolina, USA)," *Estuarine Coastal and Shelf Science*, Vol. 72, pp. 63-80 (2007).
3. Carmillet, V., Brankart, J. M., Brasseur, P., Drange, H., and Evensen, G., "A singular evolutive extended Kalman filter to assimilate ocean color data in a coupled physical-biochemical model of the North Atlantic," *Ocean Modelling*, Vol. 3, pp. 167-192 (2001).
4. Fasham, M. J. R. and Evans, G. T., "The use of optimization techniques to model marine ecosystem dynamics at the JGOFS station at 47° N 20° W," *Philosophical Transaction of the Royal Society of London B*, Vol. 348, pp. 203-209 (1995).
5. Fennel, K., Losch, M., Schroer, J., and Wenzel, M., "Testing a marine ecosystem model: sensitivity analysis and parameter optimization," *Journal of Marine Systems*, Vol. 28, pp. 45-63 (2001).
6. Friedrichs, M. A. M., "A data assimilation marine ecosystem model for the central equatorial Pacific: numerical twin experiments," *Journal of Marine Research*, Vol. 59, pp. 859-894 (2001).
7. Gerritsen, H., De Vries, H., and Philippart, M., "The Dutch continental shelf model. Quantitative skill assessment for coastal ocean models," *Coastal Estuarine Studies*, Vol. 47, pp. 425-468 (1995).
8. Hakanson, L., "The role of characteristic coefficients of variation in uncertainty and sensitivity analyses, with examples related to the structuring of lake eutrophication models," *Ecological Modelling*, Vol. 131, pp. 1-20 (2000).
9. Hemmings, J. C. P., Srokosz, M. A., Challenor, P., and Fasham, M. J. R., "Assimilating satellite ocean-colour observations into oceanic ecosystem models," *Philosophical Transaction of the Royal Society of London A*, Vol. 361, pp. 33-39 (2003).
10. Hemmings, J. C. P., Srokosz, M. A., Challenor, P., and Fasham, M. J. R., "Split-domain calibration of an ecosystem model using satellite ocean colour data," *Journal of Marine Systems*, Vol. 50, pp. 141-179 (2004).
11. Hornik, K., Stinchcombe, M., and White, H., "Multilayer feedforward networks are universal approximators," *Neural Networks*, Vol. 2, No. 5, pp. 359-475 (1988).
12. Lawson, L. M., Hofmann, E. E., and Spitz, Y. H., "Time series sampling

and data assimilation in a simple marine ecosystem model," *Deep Sea Research II*, Vol. 43, Nos. 2-3, pp. 625-651 (1996).
13. Lawson, L. M., Spitz, Y. H., Hofmann, E. E., and Long, R. B., "A data assimilation technique applied to a predator-prey model," *Bulletin of Mathematical Biology*, Vol. 57, pp. 593-617 (1995).
14. Li, M. C., Liang, S. X., and Sun, Z. C., "Application of artificial neural networks to tide forecasting," *Journal of Dalian University of Technology*, Vol. 47, No. 1, pp. 101-105 (2007). (in Chinese)
15. Liu, J. G., Liu, J. H., and Guo, H. G., "Study on parametric recognition & comparison of improved S-P model," *Journal of Changchun Normal University*, Vol. 25, No. 6, pp. 16-21 (2006). (in Chinese)
16. Losa, S. N., Kivman, G. A., and Ryabchenko, V. A., "Weak constraint parameter estimation for a simple ocean ecosystem model: what can we learn about the model and data?" *Journal of Marine Systems*, Vol. 45, pp. 1-20 (2004).
17. Losa, S. N., Vézina, A., Wright, D., Lu, Y. Y., Thompson, K., and Dowd, M., "3D ecosystem modelling in the North Atlantic: relative impacts of physical and biological parameterizations," *Journal of Marine Systems*, Vol. 61, pp. 230-245 (2006).
18. Ma, Z. P. and Jing, A. Q., "Data assimilation method applied in marine scienceits significance, system configuration and development situation," *Coastal Engineering*, Vol. 24, No. 4, pp. 83-99 (2005). (in Chinese)
19. Malve, O., Laine, M., Haario, H., Kirkkala, T., and Sarvala, J., "Bayesian modeling of algal mass occurrences using adaptive MCMC methods with a lake water quality model," *Environmental Modeling & Software*, Vol. 22, pp. 966-977 (2007).
20. McCulloch, W. S. and Pitts, W., "A logical calculus of the ideas immanent in nervous activity," *Bulletin of Mathematical Biology*, Vol. 5, pp. 115-133 (1943).
21. Minns, A. W. and Hall, M. J., "Artificial neural networks as rainfall-runoff models," *Hydrological Science Journal*, Vol. 41, No. 3, pp. 399-417 (1996).
22. Nakastuji, K., Yamanaka, R., and Nishida, S., "Numerical simulation of seasonal baroclinic circulation and dispersion process of COD in the Bohai Sea," *The First Asian and Pacific Coastal Engineering Conference*, Dalian University of Technology Press, Dalian, China. pp. 369-378 (2001).
23. Platt, T., Caverhill, C., and Sathyendranath, S., "Basin-scale estimates of oceanic primary production by remote sensing: the North Atlantic," *Journal of Geophysical Research*, Vol. 96, pp. 15147-15159 (1991).
24. Rumelhart, D. E., Hinton, G. E., and Williams, R. J., "Learning representations by back propagating errors," *Nature*, Vol. 323, pp. 533-536 (1986).
25. Seo, Dong-II and Canale, R. P., "Performance, reliability and uncertainty of total phosphorus models for lakes—I: deterministic analyses," *Water Research*, Vol. 30, pp. 83-94 (1996).
26. Shastry, J. S., Fan, L. T., and Erickson, L. E., "Nonlinear parameter estimation in water quality modeling," *Journal of the Environmental Engineering Division*, ASCE, Vol. 99, No. 3, pp. 315-331 (1973).
27. Solomatine, D. P., "Data-driven modelling: paradigm, methods, experiences," *Proceedings of the 5th International Conference on Hydroinformatics*, IWA Publishing, Cardiff, London, UK, pp. 757-763 (2002).
28. Vallino, J. J., "Improving marine ecosystem models: use of data assimilation and mesocosm experiments," *Journal of Marine Research*, Vol. 58, pp. 117-164 (2000).
29. Yang, M. D., Sykes, R. M., and Merry, C. J., "Estimation of algal biological parameters using water quality modeling and SPOT satellite data," *Ecological Modeling*, Vol. 125, pp. 1-33 (2000).
30. Zhang, M. Y., "Estimation method of oxygen consumption coefficient K1 in the water quality model," *Water Resources & Hydropower of Northeast*, Vol. 22, No. 250, pp. 42-44 (2005). (in Chinese)